25th ABCM International Congress of Mechanical Engineering
October 20-25, 2019, Uberlândia, MG, Brazil

COBEM2019-1463
NUMERICAL INVESTIGATION OF A TRANSVERSE JET IMPINGING IN AN ANNULAR FLOW

Thiago H. T. Eduardo
Luiz Fernando B. Nardi
Igor B. de Paula
Arthur M. B. Braga
Angela O. Nieckele
Department of Mechanical Engineering, Pontifícia Universidade Católica do Rio de Janeiro, 22451-900, Rio de Janeiro, RJ, Brazil
thiagohanderson@gmail.com, lfbnardi@gmail.com; igordepaula@puc-rio.br; abragra@puc-rio.br; nieckele@puc-rio.br

Abstract. *Transverse jet flow impinging in annular flow is a configuration commonly found in gas injection wells. Along those wells, hydraulic lines can be found, and its operational life can be reduced due to induced flow vibration. The geometry selected here to mimic this problem is given by an impinging jet confined in the annular space between two concentric pipes. In present work the flow field was examined with numerical simulations using OpenFOAM. Two turbulence models were tested aiming to identify the most adequate one to the problem of interest. The turbulence models tested were the realizable* $\kappa - \varepsilon$ *and the SST* $\kappa - \omega$*. Comparison with available experimental data have showed that a reasonable agreement could be obtained, with equivalent results of the two models.*

Keywords: *turbulence, impinging jet, realizable* $\kappa - \varepsilon$ *and SST* $\kappa - \omega$ *turbulence model, OpenFOAM*

1. INTRODUCTION

Flow induced vibration is a topic that has attracted attention in the last years mainly because structures are becoming lighter and materials are supporting more stress. Pressure fluctuations due to turbulence can anticipate failure in different types of equipment. As a natural consequence, the knowledge about the flow field and how it excites the vibration modes of equipment is an important subject.

Production or injection wells have hydraulic lines for control, and flow turbulence can produce vibration, reducing its operational life. This type of configuration can be approximated by a transverse flow in an annular flow, which is the focus of the present work.

Studies of flow of impinging jets on plane and curved surfaces have being conducted for a while (Gardon, 1965; Hrycak, 1981; Weigand, 2011; Molana, 2013). Several experimental works in the literature are devoted to characterize impinging jets on concave surfaces (Cornaro, 1999; Hashiehbaf, 2015). Cornaro (1999) have shown that the distance of the jet nozzle to the concave surface can have a significant influence on vortex shedding at the jet exhaust. This can change drastically the momentum and heat transfers related with the jets. Therefore, the characteristics of the jets are relevant also for the design of flow mixers, or colling/heating devices.

Recently, some experimental work employing PIV has also been conducted (Zhang, 2016; Khayrullina, 2017, Nardi and de Paula, 2018). Nardi and de Paula (2018) have gathered velocity and turbulence data for impinging jets into an annular cavity for various configurations.

Numerical simulations of this problem are scarce in the literature. Poitras *et al.* (2017) have numerically studied a jet impinging on a concave surface and have also found that the distance from the jet to the surface played a very important role in the flow characteristics.

At the present work a numerical investigation of the flow examined experimentally by Nardi and de Paula (2018) is performed, with the open source frame platform OpenFoam. The Reynolds averaged turbulence model is employed to obtained the flow field. To define the most adequate turbulence model to predict the flow of interest, the solution was obtained with the realizable κ–ε and $SST\ \kappa - \omega$ turbulence models. This work also aims to further exam the flow, providing more detailed data to enhance the previous experimental investigation.

2. MODELLING

The configuration under consideration consists of two pipes, one inside the other, with one opening at the center of the pipe, connecting the flow from the inner pipe to the annular pipe, as shown in Fig. 1. The diameter of the opening connecting the inner tube to the annular space is d_j. The flow enters the inner pipe, which has its extremity blocked, and leaves through both ends of the annular pipe to a large ambient with constant pressure, p_{amb}.

In order to compare numerical results with experimental data the same coordinate system (shown in Fig. 1) employed

by Nardi and de Paula (2018) was defined, where *x* is in the radial axis centered in the opening and *y* is the axial axis with zero located at the outside wall of the inner pipe. *L* is defined as the length of the gap between the two pipes. The inner pipe and outer diameters are D_{in} and D_{out}, respectively. The inner pipe wall thickness is *e* and the pipe length (domain length) is L_{total}.

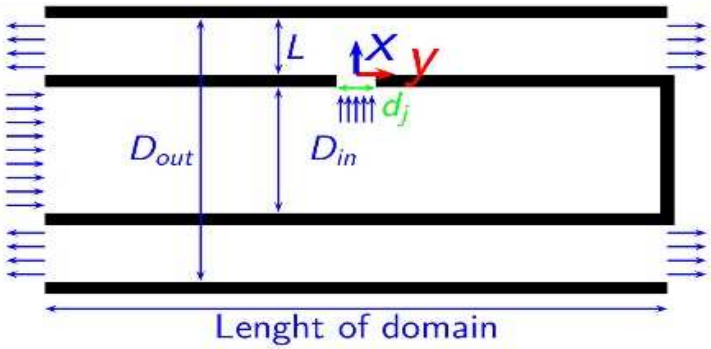

Figure 1. Schematization of the annular pipe.

To determine the turbulent flow inside the device, the following hypothesis were considered: steady state, isothermal, Newtonian fluid, incompressible and with constant viscosity flow. To model the turbulent flow, the RANS approach with the $\kappa - \varepsilon$ two equation model was selected, since the Reynolds number is very high. The conservation equations of mass and momentum are

$$\frac{\partial u_i}{\partial x_i} = 0 \tag{1}$$

$$\frac{\partial \rho u_j u_i}{\partial x_j} = -\frac{\partial \hat{p}}{\partial x_i} + \frac{\partial}{\partial x_j}\{(\mu + \mu_t)\, 2\, S_{ij}\} \tag{2}$$

where x_i represents each of the coordinate axes and u_i the components of the velocity vector, ρ is the density, μ is the molecular viscosity, μ_t is the turbulent viscosity and $\hat{p} = (p + 2/3\, \rho\, \kappa) - p_{amb}$ is a modified pressure relative to the ambient pressure, that includes the turbulent dynamic pressure. S_{ij} is the rate of deformation tensor

$$S_{ij} = \frac{1}{2}\left[\frac{\partial u_i}{\partial x_j} + \frac{\partial u_j}{\partial x_i}\right] \tag{3}$$

Both turbulence models selected to be investigated are based on the turbulent kinetic energy κ, however, one is based on the turbulent dissipation ε and the other on the specific dissipation ω. The turbulence viscosity of the realizable κ–ε is

$$\mu_t = C_\mu \frac{\rho\, \kappa^2}{\varepsilon} \tag{4}$$

SST $\kappa - \omega$ is a combination of the κ–ε far from the wall with the κ–ω near the wall. Its turbulent viscosity is

$$\mu_t = \frac{\rho \kappa}{\omega}\, \xi \tag{5}$$

where ξ is the blending coefficient, given by

$$\xi = \frac{1}{\max(1/\alpha^*,\ S\ F_2/(0.31\ \omega)} \tag{6}$$

with

$$\alpha^* = \alpha_\infty^* \left(\frac{\beta_i/3 + Re_t/6}{1 + Re_t/6}\right); \qquad Re_t = \frac{\rho\, \kappa}{\mu\, \omega} \tag{7}$$

The parameter β_i is obtained by blending the two models, $\beta_i = F_1\, \beta_{i,1} + (1 - F_1)\beta_{i,2}$, with $\beta_{i,1} = 0.075$ and $\beta_{i,2} = 0.0828$. In Eq. (6), S is the modulus of the rate of deformation tensor,

$$S = \sqrt{2\, S_{ij}\, S_{ij}} \tag{8}$$

and F_1 and F_2 are determined by

$$F_2 = \tanh(\Phi_2^2)\ ;\ \Phi_2 = \max\left[2\,\frac{\sqrt{\kappa}}{\beta^\star\,\omega\,y}, \frac{500\,\mu}{\rho\,y^2\,\omega}\right]\ ;F_1 = \tanh(\Phi_1^2)\ ;\ \Phi_1 = \min\left[max\left[\frac{\sqrt{\kappa}}{\beta^\star\omega y}, \frac{500\,\mu}{\rho\,y^2\,\omega}\right], \left[\frac{4\,\sigma_{\omega 2}\kappa}{CD\,y^2}\right]\right] \quad (9)$$

where $\sigma_{\omega 2} = 0.856$, $\beta^\star = 0.09$ and CD is given by the following equation:

$$\mathrm{CD} = \max\left[2\,\sigma_{\omega 2}\,\frac{1}{\omega}\,\frac{\partial \kappa}{\partial x_j}\,\frac{\partial \omega}{\partial x_j}, 10^{-20}\right] \quad (10)$$

Additional conservation equations are needed for κ and ε or κ and ω. The standard equations for these variables, available at the OpenFoam platform were solved.

Uniform velocity was prescribed at the inlet, $U_{in} = U_j\left(d_j/D_{in}\right)^2$, with turbulence intensity equal to 5% of mean flow kinetic energy. Turbulent dissipation equal to $\varepsilon = c_\mu^{0.75}\,\kappa^{1.5}/L_{mix}$, with $L_{mix} = 0.1D_{in}$, was imposed at the inlet for realizable $\kappa - \varepsilon$ model, and for SST $\kappa - \omega$ model $\omega = \sqrt{k}/(0.09L_{mix})$. Non-slip boundary conditions are prescribed at the solid surfaces (with the standard wall law of turbulence for the $\kappa - \varepsilon$ model) and prescribed zero relative pressure at outlets.

The flow is governed by several geometric parameters of the annular jet and the jet Reynolds number,

$$Re = \frac{\rho\,U_j d_j}{\mu} \quad (11)$$

where d_j is the diameter of the opening connecting the inner tube to the annular space, and U_j is the jet velocity through the opening.

The conservation equations were discretized with the upwind scheme to treat the convective terms with linear scheme for all other terms. Pressure velocity coupling was solved with the PISO algorithm (Verteege and Mallasekera, 1995). To guarantee that the steady state regime had been achieved, the maximum velocity at the orifice was controlled, and convergence was attained when variation was inferior to 0.2%.

A non-uniform mesh was defined, concentrated near the hole connecting both pipes. To define the number of points, a grid convergence test was carried out. The chosen variable to defined the mesh was the maximum velocity of the jet at the orifice exit. Results for this test are shown in Table 1, where it can be seen a variation of 1.3% of the maximum velocity, with the increase of the number of grid points. Note that a significant increase in the number of points were employed as shown in Table 1. Thus, the intermediate mesh size with 6.3×10^5 points was defined in the computational domain for all tests.

Number of mesh points, N_i	N_i/N_{i-1}	V_{max_i}/U_j	$V_{max_i}/V_{max_{i-1}}$
220049	–	3.10	–
631338	2.9	3.13	0.97%
3674944	6.8	3.09	1.28%

Table 1. Mesh test. Maximum velocity at the orifice.

3. RESULTS

The flow field was determined with the same geometric parameters of Nardi and de Paula (2018) experimental apparatus, so that the data could be compared. The chosen geometry was: $L/d_j = 1.7323$, $d_j/D_{in} = 0.4535$, $D_{out}/D_{in} = 0.1512$, $L_{total}\ /\ d_j = 47.25$. Further, the jet Reynolds number was set equal to Re=13924.

Figure 2 presents a qualitative comparison of the numerical results obtained with the experimental data of Nardi and de Paula (2018). At Fig. 2, iso-contours of the dimensionless velocity magnitude in the annular region, near the opening are shown, in terms of the *x-y* coordinate system represented in Fig. 1. The experimental result shown in Fig. 2(a) are mean values for 1000 samples (this sample size was chosen to guarantee statistically steady state results), while the numerical results correspond to the steady state solution.

Examining Figs. 2 (a-c), it can be seen that the high velocity jet is tilted to the right side of the annular pipe, it impinges at the outer diameter, and the flow is unevenly distributed in both directions with a boundary layer being formed along the outer wall. Note that both turbulent models predict very similar flow field, with higher velocities to the right near the outer radius than the experimental data. The maximum normalized velocities is 1.6 for realizable $\kappa - \varepsilon$ and 1.5 for $SST\ \kappa - \omega$, while only 1.2 for experimental. Both models also predict a reflection of the impinging jet to the interior of the annular gap to the left, while a very mild inclination to the center is seen from the experimental result. Nevertheless, very good agreement was obtained with both models.

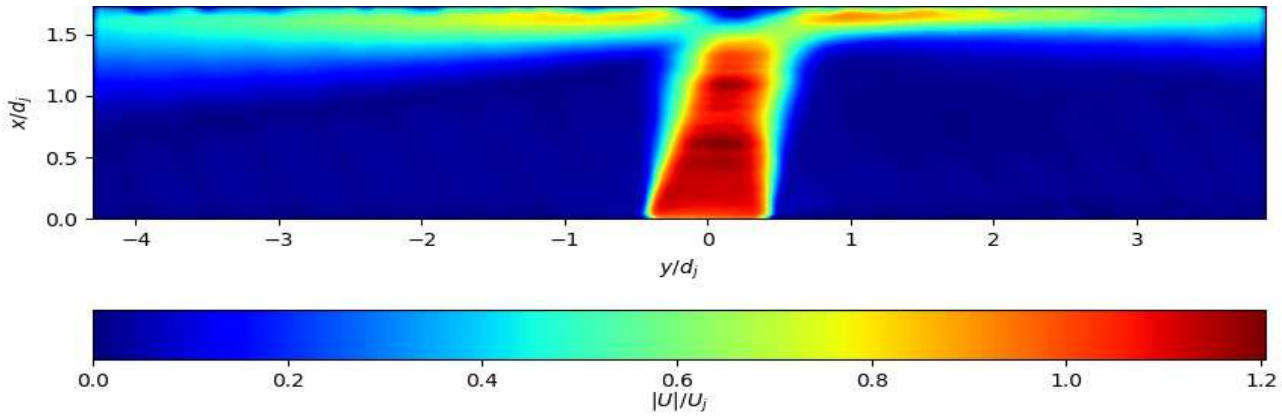

(a) experimental: PIV

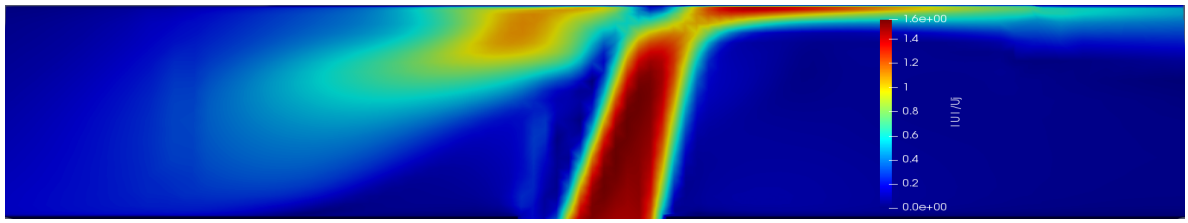

(b) numerical realizable $\kappa - \varepsilon$ results

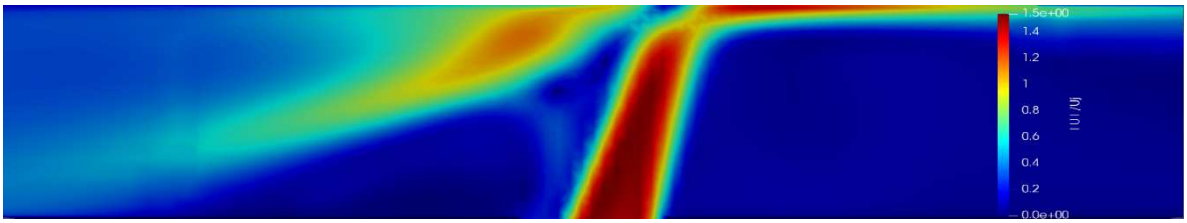

(c) numerical $SST\ \kappa - \omega$ results

Figure 2. Velocity magnitude contours through the connecting opening. Numerical versus experimental.

A quantitative comparison between experimental and numerical data for the radial velocity component is shown in Fig. 3, corresponding to the realizable $\kappa - \varepsilon$ and SST $\kappa - \omega$ simulations. The experimental results were obtained with PIV, by using a laser plane. Assuming that the laser plane was exactly centered at the orifice, the numerical results were taken from this plane. The velocity profile along axial direction for several radial positions inside the annular gap are shown. Each profile is normalized by the mean jet velocity at the exit of the opening ,U_J. Two additional lines passing by the position of the maximum of each profile are also included to aid analyzing the results. One line corresponds to the experimental data and the other corresponds to the numerical result.

Analyzing Fig. 3, it can be seen that the experimental profile is almost uniform as it leaves the orifice, and it diffuses as the radial coordinate increases. Similar profiles were numerically obtained, however, the maximum velocity is larger. A diffusion of the jet for larger radial coordinates was also numerically obtained. Analyzing the velocity profiles, one can see that the numerical results show a recirculation zone on the left side of the orifice, which induces a stronger shift of the jet, and increases the jet velocity, so that mass conservation is attained. Note also that the presence of recirculation in the hole exit affects the velocity profile at different positions along the gap. It can be seen that realizable $\kappa - \varepsilon$ and SST $\kappa - \omega$ have very similar results and both can be applied to study this type of configuration.

Aiming to understand the flow field and to explain the differences between the numerical and experimental results, different views of the flow are examined in Figs. 4 and 5.

Figure 4 shows the dimensionless magnitude of the velocity field at the frontal central plane passing by the connecting opening, obtained with SST $\kappa - \omega$ model. This plane was not investigated by Nardi and de Paula (2018), and it passes by $y/d_j = 0$, and it is normal to the axis of the pipes. It can be seen in Fig. 4 that the fluid is accelerated in the radial direction even inside the inner pipe, i.e., before entering the orifice. The strong curvature to enter the hole to form the jet induces a recirculation near the hole. The jet impingement at the outer radius is also clearly seen, with the flow splitting along the outer pipe, flowing in the angular direction. It is interesting to observe the jet splitting even before reaching the outer wall. The jet splitting is due to the high pressure at the impinging region and lower pressure at the annular extremities.

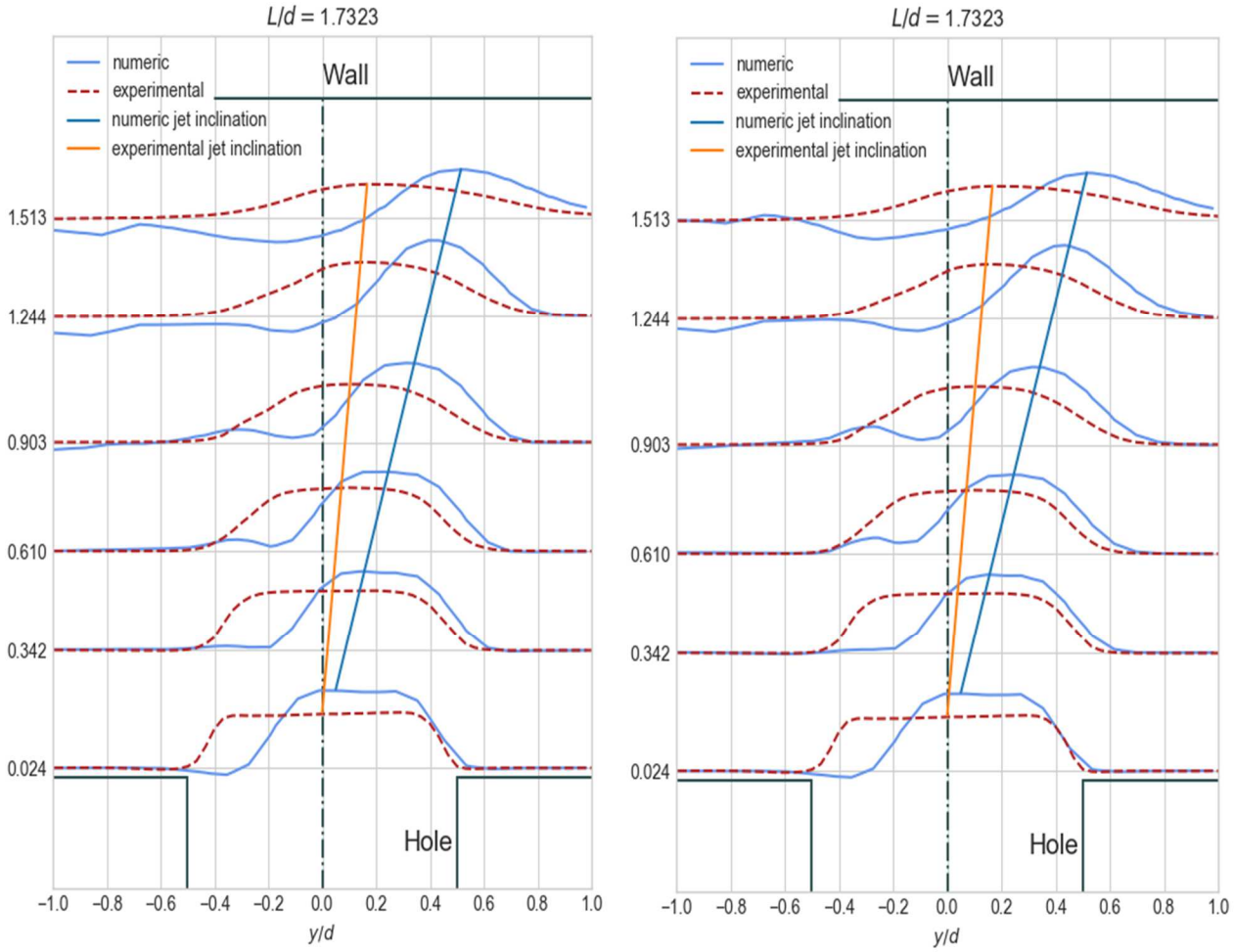

(a)Realizable $\kappa - \varepsilon$ (b) SST $\kappa - \omega$

Figure 3. Radial velocity profile along distance through jet opening. Numerical versus experimental data.

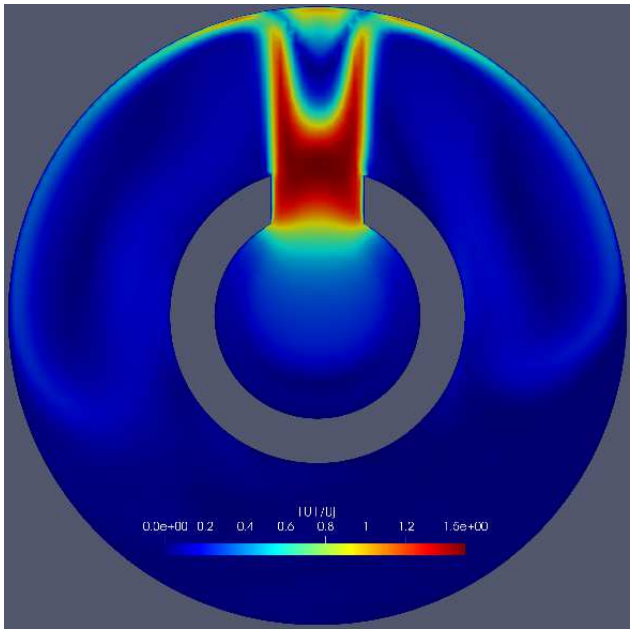

Figure 4. Dimensionless velocity magnitude contours through the frontal central plane passing by the connecting opening (SST $\kappa - \omega$ model).

In order to better illustrate the three-dimensional characteristics of the jet, Fig. 5 shows an iso-surface of dimensionless velocity magnitude equal $|U|/U_j = 1$. It is possible to observe that flow distribution is very complex. High flow velocities are seen inside the inner pipe. Furthermore, the jet inside the annular region does not have a circular shape, it is inclined to the right and it presents a depression in the left side. Finally, the spread of the fluid along the outer radius, in both axial and angular directions is clearly seen. It is also possible to notice that there exists a split of fluid in the opposite direction to the jet inclination. This split is very thin and coplanar to the plane chosen by Nardi and de Paula (2018).

Note that a very small deviation of the central plane might reflect on variations of the radial velocity component. Thus, a possible explanation for the difference among the experimental and numerical results might be that the data was not obtained exactly at the same plane by the two methodologies.

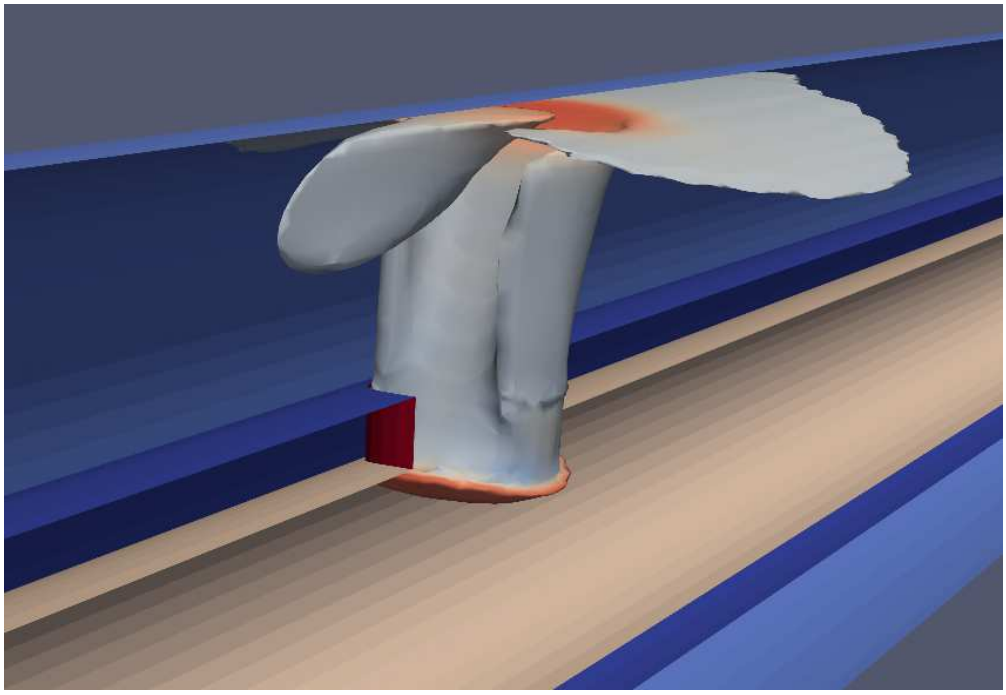

Figure 5. Iso-surface of dimensionless velocity magnitude $|U|/U_j = 1$ near the connecting opening (SST $\kappa - \omega$ models).

4. CONCLUSION

The flow field of a transverse jet impinging in an annular flow was numerically investigated. A comparison of the numerically determined flow field, employing the realizable $\kappa - \varepsilon$ and SST $\kappa - \omega$ models presented similar result when compared to experimental data. Both turbulence models lead to similar results with SST $\kappa - \omega$ been slightly better.

A small deviation of the numerical result and experimental data might be explained by the highly 3D flow structure through the orifice, i.e., very small differences at the plane positioning to compare the results may not capture the presence of recirculation near the orifice.

The present results indicate that this model can be applied to further investigate the problem, considering others opening communications between the pipes, as well as a more realistic configuration of an actual valve. Further tuning of the model can be achieved with a broader comparison with other experimental data.

5. ACKNOWLEDGEMENTS

The authors are thankful for the financial support of Petrobras in the development of this research project. The authors also thank CNPq and CAPES for the continuous support.

6. REFERENCES

Cornaro, C., Fleischer, A.S., Goldstein, R.J., 1999. “Flow visualization of a round jet impinging on cylindrical surfaces”. *Exp. Therm. Fluid Sci.*Vol. 20, pp.66–78.

Gardon, R.; Akfirat, J. C., 1965. “The role of turbulence in determining the heat-transfer characteristics of impinging jets”, *International Journal of Heat and Mass Transfer*, Vol. 8\:10, pp.1261-1272.

Hashiehbaf, A., Baramade, A., Agrawal, A. Romano, G.P., 2015. "Experimental investigation on an axisymmetric turbulent jet impinging on a concave surface", *International Journal of Heat and Fluid Flow*, Vol. 53, pp. 67-182.

Hrycak, P., 1981, "Heat transfer from a row of impinging jets to concave cylindrical surfaces", *International Journal of Heat and Mass Transfer*, Vol. 24, pp..407-419.

Khayrullina, A., van Hooff, T., Blocken, B. and van Heijst, G.J.F., 2017. "Piv measurements of isothermal plane turbulent impinging jets at moderate Reynolds numbers". Experiments in Fluids, Vol. 58, No. 4, p. 31.

Molana, M., Banooni, S., 2013 Verteege, "Investigation of heat transfer processes involved liquid impingement jets: a review", *Brazilian Journal of Chemical Engineering*, Vol. 30, pp.413-435.

Nardi, L.F.B., de Paula, I. B., 2018, "Experimental characterization of outward annular impinging jets", *Proc. 17th Brazilian Congress of Thermal Sciences, and Engineering*. ENCIT-2018-682.

Poitras, G. J., Babineau, A., Roy, G., Brizzi, E.-E, 2017, "Aerodynamic and heat transfer analysis of a impinging jet on a concave surface", *International Journal of Thermal Sciences*, Vol. 114, pp.184-195.

Verteege, H. K. and Malalasekera, W. 1995, *An Introduction to Computational Fluid Dynamics. The Finite Volume Method*, Logman Scientifc & Technical.

Weigand, B., Spring, S., 2011. "Multiple Jet Impingement- A Review", *Heat Transfer Research*, Vol. 42, pp. 101-142

Zhang, J., Liu, Y., Qi, G., Jiao, W. and Yuan, Z., 2016. "Flow characteristics in free impinging jet reactor by particle image velocimetry (piv) investigation". Fluid Dynamics Research, Vol. 48, p. 045505.

OpenFoam User Guide. https://www.openfoam.com/documentation/.

7. RESPONSIBILITY NOTICE

The authors are the only responsible for the printed material included in this paper.